HHS Public Access

Author manuscript

Nat Neurosci. Author manuscript; available in PMC 2015 November 01.

Published in final edited form as:

Nat Neurosci. 2015 May ; 18(5): 674–682. doi:10.1038/nn.3990.

GABAergic regulation of cerebellar NG2-cell development is altered in perinatal white matter injury

Marzieh Zonouzi[1,2], **Joseph Scafidi**[1,3], **Peijun Li**[1], **Brian McEllin**[1], **Jorge Edwards**[1], **Jeffrey L. Dupree**[4], **Lloyd Harvey**[5], **Dandan Sun**[5], **Christian A. Hübner**[6], **Stuart G. Cull-Candy**[2], **Mark Farrant**[2], and **Vittorio Gallo**[1]

[1]Center for Neuroscience Research, Children's Research Institute, Children's National Medical Center, Washington, DC 20010, USA

[2]Department of Neuroscience, Physiology and Pharmacology, University College London, London WC1E 6BT, UK

[3]Department of Neurology, Children's National Medical Center, Washington, DC 20010, USA

[4]Department of Anatomy and Neurobiology, Virginia Commonwealth University, Medical Center, Richmond, Virginia 23298, USA

[5]Department of Neurology, University of Pittsburgh, Pittsburgh, PA 15213, USA

[6]Friedrich-Schiller-University Jena, Institute of Human Genetics, Jena University Hospital, Jena, Germany

Abstract

Diffuse white matter injury (DWMI), a leading cause of neurodevelopmental disabilities in preterm infants, is characterized by reduced oligodendrocyte formation. Oligodendrocyte precursor cells (NG2-cells) are exposed to various extrinsic regulatory signals, including the neurotransmitter GABA. We investigated GABAergic signaling to cerebellar white matter NG2-cells in a mouse model of DWMI (chronic neonatal hypoxia). We found that hypoxia caused a loss of $GABA_A$ receptor-mediated synaptic input to NG2-cells, extensive proliferation of these cells and delayed oligodendrocyte maturation, leading to dysmyelination. Treatment of control mice with a $GABA_A$ receptor antagonist or deletion of the chloride-accumulating transporter NKCC1 mimicked the effects of hypoxia. Conversely, blockade of GABA catabolism or GABA uptake reduced NG2-cell numbers and increased the formation of mature oligodendrocytes both in control and hypoxic mice. Our results indicate that GABAergic signaling regulates NG2-cell differentiation and proliferation *in vivo*, and suggest that its perturbation is a key factor in DWMI.

Correspondence to: Stuart G. Cull-Candy; Mark Farrant; Vittorio Gallo.

Author contributions

MZ, JS, SGC-C, MF and VG designed the experiments. MZ and PL performed the electrophysiology. MZ and JS carried out the immunocytochemistry and drug treatment studies. JS and VG generated the *Pdgfra-creER*^{T2};*Nkcc1*$^{fx/fx}$;*Rosa26-yfp* mouse. MZ, JS and JLD performed electron microscopy. BM performed culture experiments. GE performed genotyping. LH and DS provided the *NKCC1*$^{-/-}$ mouse brain tissue. CAH provided the *Nkcc1*$^{fx/fx}$ mice. MZ, JS and MF analyzed the experimental data. MZ and MF prepared the figures and wrote the manuscript, with contributions from SGC-C, JS and VG.

Introduction

Infants born prematurely (23 to 32 weeks gestation) are at high risk of developing diffuse white matter injury (DWMI), which is often linked to chronic hypoxia[1,2]. DWMI, also known as bilateral periventricular leukomalacia, is a leading cause of long-term neurological damage, which is manifest as behavioral, cognitive or motor defects[3,4]. DWMI is associated with severely disrupted development of the sub-cortical white matter[5], and has been linked to loss of late NG2-expressing oligodendrocyte progenitor cells (NG2-cells)[6,7].

DWMI in preterm infants is associated with reduced expression of GABAergic markers in the cortex, subplate, and white matter[8], and recent studies have identified a reduction in cortical GABA in a clinically relevant mouse model of DWMI[9]. GABA is recognized as a critical regulator of neuronal development and restricts the proliferation of embryonic and adult neuronal precursor cells[10,11] and glial fibrillary acidic protein-positive ($GFAP^+$) subventricular zone stem cells[12,13]

In recent studies, neonatal hypoxia has been shown to enhance Notch signaling and down-regulate the cell cycle arrest protein p27(Kip1) in NG2-cells, contributing to their disrupted developmental progression and the dysmyelination of sub-cortical white matter[14,15]. Enhancing NG2-cell proliferation and maturation results in improved functional outcomes[15]. NG2-cells express $GABA_A$ receptors and receive GABAergic synapses from interneurons early in development[16,17]. Thus, GABAergic signaling during cell cycle progression could provide a mechanism for controlling the proliferation and differentiation of NG2-cells into mature oligodendrocytes, in an activity-dependent manner.

Here we examined GABAergic regulation of NG2-cell development in cerebellar white matter. Several studies have identified disrupted cerebellar development as a common feature of brain injury in preterm infants[18–21], yet the underlying mechanisms are relatively unexplored. The cerebellum is important not only for motor coordination and motor learning, but also for cognitive function[22,23], suggesting that cerebellar abnormalities in infants with DWMI might contribute to the development of cognitive and affective disturbances[24].

In an established mouse model of chronic hypoxia, which reproduces key features of DWMI[6,25,26], we observed delayed Purkinje cell maturation and disrupted cerebellar development. These changes were associated with dysmyelination, extensive proliferation of NG2-cells and a loss of mature oligodendrocytes. We also observed a loss of $GABA_A$ receptor-mediated synaptic input to NG2-cells from local white matter interneurons. The effects of hypoxia on oligodendrocyte lineage cells were mimicked by blockade of $GABA_A$ receptors or deletion of the chloride-accumulating transporter NKCC1, and reversed by inhibition of GABA catabolism or uptake. Together, these findings suggest that GABA, acting through $GABA_A$ receptors, regulates cerebellar NG2-cell development and that this is altered in a model of diffuse white matter injury.

Results

Neonatal hypoxia disrupts myelination in the cerebellum

To study the effect of hypoxia on the GABAergic regulation of NG2-cells and myelination in cerebellar white matter we used a mouse model of DWMI[6,25,26]. Mice in which oligodendrocyte lineage cells expressed DsRed (NG2DsRed mice) were exposed to hypoxic conditions (10.5% O_2) from P3 to P11. Initially, we examined cerebellar sections from mice at four time points; mid way through the hypoxic treatment (P7), immediately following the treatment (P11), and at two ages following return to normoxic conditions (P15 and P30) (Fig. 1a). Neonatal hypoxia led to changes in cerebellar gross anatomy and cellular development. Specifically, following the hypoxic treatment (P11) there was a reduction in cerebellar size, coupled with structural changes, including a poorly developed intercrural fissure separating cerebellar lobules VI and VII (Supplementary Fig. 1). At P11 these changes were associated with a reduction in thickness of the molecular layer and a thickening of the external germinal layer (Fig. 1b).

Purkinje cells are GABAergic neurons that provide the sole output of the cerebellar cortex. Immunofluorescence for a Purkinje cell marker, calbindin, revealed that hypoxic treatment led to pronounced changes in dendritic extent and arborization at P7-15 without any change in Purkinje cell number (Fig. 1c–d and Supplementary Fig. 2a). Purkinje cell dendritic length recovered to control values at P30 (Fig. 1e).

Immunolabeling with antibodies against markers for neurofilament (NF200) and myelin basic protein (MBP) suggested a reduction in the number of myelinated axons in the granule cell layer and white matter (Fig. 1f–h, and Supplementary Fig. 2b). At P11 and P15 the loss of MBP labeling persisted when immunofluorescence was normalized to that of NF200, suggesting hypomyelination rather than axonal loss alone. Importantly, hypoxia did not increase apoptosis or axonal damage (Supplementary Fig. 2c–e). At P30 the MBP/NF200 ratio was not reduced by hypoxia (data not shown). These observations were supported by western blot data; the MBP/NF200 ratio was reduced at P11 (from 0.80 ± 0.09 to 0.39 ± 0.09, $t_{3.97} = 3.25$ $P = 0.032$) but not at P30 (1.06 ± 0.22 versus 0.73 ± 0.16, $t_{1.226} = 3.65$ $P = 0.29$; both $n = 3$; Welch two-sample unpaired *t*-test) (Supplementary Fig. 3a,b). Although these data suggest partial recovery with age, electron microscopy provided direct evidence for hypomyelination, with increased *g* ratios at both P11 and P30 (Fig. 1i,j and Supplementary Fig. 3c,d). Together the results indicate disrupted cerebellar axonal myelination following neonatal hypoxia.

Neonatal hypoxia delays the development of NG2-cells

We next investigated whether the loss of axonal MBP following neonatal hypoxia was a result of abnormalities in the development of NG2-cells, as has been described previously for subcortical white matter[6,14]. We examined the proliferation and maturation of NG2-cells in the cerebellar white matter by labeling cells for the oligodendroglia marker Olig2, the cell cycle marker Ki67 and the mature oligodendrocyte marker CC1 (Fig. 2a,b). Neonatal hypoxia led to an increase in the number of $Olig2^+$ NG2-cells (oligodendrocyte progenitors),

an increase in the number of Ki67$^+$ NG2-cells (proliferating NG2-cells) and a decrease in the number of CC1$^+$ cells (mature oligodendrocytes) at P7, 11, 15 and 30 (Fig. 2c).

Confirming the increase in NG2-cell proliferation following hypoxia, at P11 we observed an increase in the number of oligodendrocyte precursor cells identified with PDGFαR (platelet-derived growth factor-α receptor) that were positive for the cell cycle marker BrdU (bromodeoxyuridine) (from 13.2 ± 2.1 to 37.4 ± 3.6 cells per 10^6 μm^3, $t_{5.95} = 4.96$, $P = 0.0019$, $n = 5$ normoxic and 4 hypoxic mice; Welch two-sample unpaired t test). In addition, western blot analysis revealed a corresponding decrease at P7, 11, 15 and 30 in the level of the mature oligodendrocyte marker CNPase (2′,3′-cyclic nucleotide-3′-phosphodiesterase) (Supplementary Fig. 4). At P60 we identified a recovery in the number of NG2- and CC1$^+$ cells in the cerebellar white matter (Fig. 2c), suggesting a delay in maturation of NG2 cells following hypoxia rather than a persistent block of differentiation.

Decreased Purkinje cell firing following neonatal hypoxia

The proliferation of NG2-cells and their differentiation into myelinating oligodendrocytes has been shown to depend on the activity of neighboring axons[27,28]. Indeed, NG2-cells in both in gray and white matter receive glutamatergic and GABAergic synaptic input from neurons[16,17,29–31]. Previous studies have reported a loss of GABAergic neurons in the cortical white matter of preterm infants with white matter damage[8], and delayed interneuron maturation and decreased GABA content in the cortex of mice following perinatal hypoxia[9]. We therefore investigated whether alterations in the development of white matter NG2-cells following neonatal hypoxia could reflect a reduced GABAergic ‘input’ from neurons.

First, as Purkinje cell axons have been suggested as a potential source of IPSCs recorded from NG2-cells in the white matter of the developing cerebellum[32], we asked whether the changes in the morphology of Purkinje cells following neonatal hypoxia were accompanied by changes in their activity. Using cell-attached recordings in acute slices (P10-11), we observed a clear shift in the pattern of Purkinje cell simple spike firing (Supplementary Fig. 5). The mean frequency of firing was reduced to <50% of that seen in slices from normoxic mice, indicating a marked change in this potential source of GABAergic input to cerebellar NG2-cells.

Loss of cerebellar interneurons following neonatal hypoxia

Next, using GAD65-GFP mice, we examined the effect of neonatal hypoxia on the prevalence of interneurons in the cerebellar molecular layer and white matter. We found that GAD65$^+$ cells were present in both the white matter and molecular layer at P11. Unlike NG2-cells, GAD65$^+$ cells were decreased in number by neonatal hypoxia (Fig. 3a–d).

Additionally, we examined the prevalence of GAD65$^+$ interneurons expressing the transcription factor Pax2. We observed a striking reduction in the number of Pax2$^+$/GAD65$^+$ cells in the white matter following hypoxia (Fig. 3e,f), suggesting a selective loss of differentiating interneuron progenitors[33]. Consistent with this, at P11 (72 hours following BrdU injection at P8) we observed a decrease in the proportion of BrdU$^+$/GAD65$^+$ interneurons in the white matter of hypoxic mice (Supplementary Fig. 6). An even more

pronounced decrease was observed in the molecular layer, suggesting a potential deficit in proliferation. The hypoxia-induced decrease in the number of white matter interneurons was not associated with any increase in apoptosis (Supplementary Fig. 2d). These data suggest that hypoxia results in a loss of this potential source of GABAergic input to cerebellar NG2-cells.

Reduced GABAergic input to NG2-cells and interneurons

To determine the source of GABAergic input to cerebellar NG2-cells, we performed whole-cell recordings from white matter NG2-cells at P7-8. In the presence of 1 μM strychnine hydrochloride, 20 μM 6,7-dinitroquinoxaline-2,3-dione (DNQX) and 20 μM D(−)-2-amino-5-phosphopentanoic acid (D-AP5) (to block AMPA, NMDA and glycine receptors) we observed spontaneous outward currents in 20 out of 31 NG2-cells recorded at +30 mV (Fig. 4a,b). When tested (in 4 cells), the currents were blocked by the $GABA_A$ receptor antagonist SR-95531 (20 μM; data not shown). Across all 31 cells from 13 mice (each recorded for 5 mins), the mean frequency of currents was low (0.08 ± 0.03 Hz). For those cells in which the number of sIPSCs was sufficient to allow a determination of their mean amplitude (13 cells with 17–50 currents each) the mean peak amplitude was 18.5 ± 3.1 pA and the $\tau_{w,\,decay}$ (see **Methods**) was 92.8 ± 11.8 ms. Although some cells had currents with average 10–90% risetimes ≤ 1ms, the mean risetime across all 13 cells was relatively slow (2.5 ± 0.6 ms), similar to that reported previously for cerebellar white matter NG2-cells in rat[32]. We found that in each of 4 NG2-cells tested, the frequency of spontaneous IPSCs was reduced by application of 1 μM TTX (normalized frequency 0.50 ± 0.12; $t_3 = -4.11$, $P = 0.026$, one sample *t* test), suggesting that IPSCs originate from neurons, and are ordinarily dependent on the activation of voltage-gated Na^+ channels. We also found that, in the presence of TTX, application of hyperosmotic sucrose increased miniature IPSC (mIPSC) frequency (Supplementary Fig. 7). Moreover, following pre-treatment of the slices with bafilomycin A1 (2 μM), a specific inhibitor of the vesicular proton pump (V-type ATPase), mIPSCs were absent (12 cells from 3 mice; data not shown). These observations provide strong support for a vesicular origin of the IPSCs in NG2-cells[34]. Importantly, neonatal hypoxia led to a marked decrease in the prevalence of NG2-cells with sIPSCs, from 65% (as described above) to 7% (2 out of 29 cells from 9 mice) (Fig. 4a,b). Across cells, the overall frequency of currents was reduced by 99% and phasic charge transfer (see **Methods**) was reduced by 75% (Fig. 4b).

The formation of GABAergic synapses between molecular layer interneurons is known to precede their morphological and neurochemical differentiation[35]. Consistent with synaptogenesis being an early step in interneuron maturation, we observed sIPSCs in almost all recordings from $GAD65^+$ neurons in the white matter at P7-8 (27 out of 31 cells from 10 mice) (Fig. 4c,d). In parallel with the disrupted GABAergic input to NG2-cells, we also observed a decrease in the prevalence of interneuron sIPSCs following hypoxia (8 out of 18 cells from 7 mice). Although there was no change in sIPSC mean amplitude or decay (peak amplitude 22.9 ± 2.5 pA to 18.8 ± 4.2 pA, $t_{5.44} = 0.70$, $P = 0.51$; $\tau_{w,\,decay}$ 52.0 ± 5.5 ms to 51.0 ± 13.7 ms, $t_{4.03} = 0.06$, $P = 0.95$; $n = 25$ and 4 cells from 3 and 10 mice, respectively; Welch two-sample unpaired *t*-test) there was a 49% decrease in the number of white matter

interneurons with sIPSCs, a 74% decrease in overall sIPSC frequency and a 68% decrease in phasic charge transfer (Fig. 4c,d).

NG2-cells are innervated by local interneurons

Carbachol, a muscarinic acetylcholine receptor agonist, has been shown to potently activate hippocampal interneurons, resulting in an increased frequency of sIPSCs in hippocampal NG2-cells[16,36]. We found that carbachol (10 μM) increased the frequency of sIPSCs in white matter NG2-cells from normoxic- but not hypoxic mice (Fig. 5a,b), consistent with a loss of presynaptic input. $GABA_A$ receptors were present in NG2-cells following hypoxia, as infrequent synaptic events were still observed (Fig. 5a) and whole-cell currents could be evoked by bath application of GABA (data not shown). Recent studies have demonstrated that carbachol can directly activate muscarinic receptors in NG2-cells[37], raising the possibility that the increase in sIPSC frequency could be independent of neuronal input. However, the loss of response following hypoxia makes this unlikely. Moreover we found that in normoxic mice the effect of carbachol was blocked by prior treatment with TTX or reversed by its subsequent application (Supplementary Fig. 7).

The effect of carbachol on sIPSC frequency appeared to reflect an increase in the synaptic input from white-matter interneurons rather than from Purkinje cells, as carbachol markedly increased the firing of $GAD65^+$ white-matter interneurons (Fig. 5b) while having no effect on the firing of Purkinje cells (Fig. 5c). In addition, electrical stimulation in the Purkinje cell layer failed to evoke IPSCs in white-matter NG2-cells, while evoking IPSCs in a majority of white matter interneurons (data not shown). Furthermore, application of the specific SK2 channel inhibitor apamin (100 nM), which produced a marked increase in Purkinje cell firing and bursting (Fig. 5d) without affecting the firing of white-matter interneurons (Fig. 5e), did not alter the frequency of sIPSCs in NG2 cells (0.034 ± 0.045 Hz to 0.053 ± 0.020 Hz, $P = 0.30$; $n = 6$ cells from 3 mice, Welch two-sample paired *t* test). Together, these results suggest that cerebellar white matter NG2-cells are innervated by local interneurons.

GABAergic signaling regulates NG2-cell development *in vivo*

We next investigated whether manipulation of GABAergic transmission *in vivo* could alter the proliferation and differentiation of NG2-cells. To do this, we initially injected NG2DsRed mice daily from P5-11 with the $GABA_A$ receptor antagonist bicuculline and examined immunolabeling for Olig2, Ki67 and CC1 in the cerebellar white matter. Treatment with bicuculline (1 mg/kg i.p.) resulted in a more than 2-fold increase in the number of $Olig2^+$ NG2-cells, a greater than 3-fold increase in the number of $Ki67^+$ NG2-cells, and a 40% decrease in the number of $CC1^+$ cells (Fig. 6a and Supplementary Fig. 8a). We also examined the effect of increasing the availability of GABA by treating mice with the GABA transporter (GAT-1) inhibitor tiagabine (50 mg/kg i.p., P5-11) or the GABA transaminase (GABA-T) inhibitor vigabatrin (100 mg/kg i.p., P5-11). In marked contrast to the effects of bicuculline, both tiagabine and vigabatrin decreased NG2-cell proliferation and increased the number of mature oligodendrocytes compared to vehicle-injected mice (Fig. 6a and Supplementary Fig. 8a).

Do these changes in NG2-cell development reflect altered $GABA_A$ receptor-mediated signaling to NG2-cells? To address this, we examined the effect of $GABA_A$ receptor drugs on the proliferation of purified cortical NG2-cells in culture (see **Methods**). Treatment with bicuculline (50 μM) did not affect NG2-cell proliferation. Conversely, the agonist muscimol (100 μM) produced a decrease in the number $BrdU^+$ NG2-cells (Supplementary Fig. 8b). Thus, $GABA_A$ receptors on NG2-cells can directly influence their proliferation.

In both neuronal and glial precursors, GABA causes depolarization due to the expression of the Na^+-K^+-Cl^- cotransporter 1 (NKCC1), which maintains an elevated intracellular chloride[13,16,38,39]. Consistent with a role for GABAergic signaling in the regulation of NG2-cells, cerebellar sections from mice deficient in NKCC1 displayed changes similar to those seen with bicuculline. Thus, at P7, 11 and 15 *NKCC1*$^{-/-}$ mice showed increased proliferation of white matter NG2-cells and decreased numbers of mature $CC1^+$ oligodendrocytes compared to littermate controls (Fig. 6b and Supplementary Fig. 9).

To determine the role of GABA-mediated depolarization in NG2-cells specifically, we crossed *Nkcc1*$^{fx/fx}$ mice with *Rosa26-yfp* reporter mice. The offspring were crossed with *Pdgfra-creER*^{T2} mice, allowing the selective knockout of NKCC1 from NG2-cells and the persistent identification of oligodendrocyte lineage cells (see **Methods**). We compared *Pdgfra-creER*^{T2};*Nkcc1*$^{fx/fx}$;*Rosa26-yfp* with littermate controls (*Pdgfra-creER*^{T2};*Nkcc1*^{fx};*Rosa26-yfp*) at P15 and determined the percentage of GFP^+ oligodendrocyte lineage cells that were positive for NG2, Ki67 or CC1, and the intensity of MBP labeling in the white matter. The selective deletion of NKCC1 from NG2-cells increased the proportion of oligodendrocyte lineage cells that expressed NG2, increased the proportion of cells that expressed Ki67, reduced the proportion of cells that expressed CC1 and reduced MBP labeling in the white matter (Fig. 6c,d). Of note, the number of $CC1^+$ GFP^+ cells in the littermate controls was not different from that seen in *Pdgfra-creER*^{T2};*Rosa26-yfp* mice (data not shown). Together these data are consistent with the idea that $GABA_A$ receptor-mediated depolarization promotes the development of cerebellar NG2-cells *in vivo*.

Vigabatrin and tiagabine ameliorate the effects of hypoxia

Next, we asked whether increasing the availability of GABA *in vivo* after hypoxia could influence the proliferation and differentiation of NG2-cells. Following hypoxic treatment (P3-11), we injected mice daily for 5 days (P11-15) with tiagabine (50 mg/kg i.p.), vigabatrin (100 mg/kg i.p.) or saline. We prepared cerebellar sections at P15 from hypoxic and normoxic drug-treated and control animals and examined immunolabeling for Olig2, Ki67 and CC1 in the cerebellar white matter. Both treatments reduced the number of $Olig2^+$- and $Ki67^+$ NG2-cells, whilst tiagabine increased the number of $CC1^+$ cells (Fig. 7a,b and Supplementary Fig. 10). Following vigabatrin or tiagabine, the number of mature oligodendrocytes was not different from that in untreated normoxic animals.

To determine whether the restoration of mature oligodendrocyte number was associated with recovery of myelination, we examined MBP immunolabelling. Following tiagabine treatment MBP expression, as determined by fluorescence intensity, was indeed increased (Fig. 7c,d). Together these data suggest that enhancing GABA availability *in vivo* following

hypoxia enhances the cellular progression of NG2-cells and promotes oligodendrogenesis and myelination.

Discussion

Using a clinical relevant *in vivo* mouse model of DWMI we have demonstrated that chronic neonatal hypoxia results in dysregulated development of cerebellar white matter NG2-cells, leading to hypomyelination. This effect was associated with disruption of GABAergic signaling from white matter interneurons to NG2-cells. In addition, we demonstrated that treatment of mice with drugs known to modify GABA levels and/or $GABA_A$ receptor-mediated signaling altered the developmental progression of NG2-cells into mature oligodendrocytes. Equivalent results were also obtained by selectively abating the Cl^- transporter NKCC1 in NG2-cells. Together, our findings suggest that reduced GABAergic synaptic transmission contributes to the cerebellar hypomyelination seen in DWMI. Our findings are relevant not only to the understanding of cerebellar maturation and the etiology of DWMI but also to the development of therapies to promote repopulation of damaged brain regions with myelinating oligodendrocytes[15].

Neonatal hypoxia disrupts cerebellar myelination

Our observation of reduced myelin formation following hypoxia echoes the decreases in cerebellar white matter volume detected in premature neonates with DWMI[21,40]. We found that neonatal hypoxia resulted in increased proliferation of NG2-cells in the cerebellar white matter and a reduction in the number of mature $CC1^+$ oligodendrocytes. In premature infants, the highest risk for DWMI is around 23–32 weeks of gestation. This time period corresponds to the onset of premyelinating oligodendrocyte production and early white matter myelination. Motor impairment and the development of cognitive defects have been linked to cerebellar damage in premature infants[21,24], and Purkinje cell abnormalities have been seen in post mortem studies of patients with autism spectrum disorders (ASDs) and in a mouse model of ASD[23]. Thus, it seems likely that the cerebellar dysmyelination seen in our model of DWMI may be of clinical significance.

Neonatal hypoxia disrupts GABAergic signaling in the cerebellar white matter

Neonatal hypoxia, in addition to disrupting the development of GABAergic Purkinje cells, caused a loss of proliferating $GAD65^+$ interneuron progenitors in the cerebellar white matter. A similar loss has been reported in mice deficient in the DNA repair factor XRCC1, an effect linked to an increase in the expression of the cell cycle arrest protein p53[41]. Moreover, loss of the cell cycle protein cyclin D2 has also been shown lead to a loss of cerebellar molecular layer interneurons[42], suggesting that control of proliferation is critical for interneuron development. Interestingly, mice lacking XRCC1 also have reduced hippocampal CNPase[41], suggesting that a reduction in GABAergic signaling could also alter the generation of mature oligodendrocytes in the hippocampus.

NG2-cells express $GABA_A$ receptors[16,39], and in the cortex[31], hippocampus[16,17,30] and cerebellum[32] these cells receive GABAergic synaptic input during the first postnatal week. Purkinje cells have been suggested to provide GABAergic synaptic input to cerebellar NG2-

cells[32]. By contrast, our recordings from cerebellar white matter NG2-cells at P7-8 suggest that they receive GABAergic synaptic input solely from local GAD65$^+$ interneurons. The sIPSCs in NG2-cells had varied rise times, suggesting that they may result both from direct synaptic contact and GABA spillover. Following neonatal hypoxia, we observed a profound a loss of GABAergic currents in cerebellar white matter NG2-cells, and disrupted differentiation of NG2-cells into mature oligodendrocytes, suggesting that GABAergic activity may regulate this process. Of note, a loss of mature oligodendrocytes has also been detected in an animal model of Rett Syndrome[43], in which GABAergic synaptic transmission is reduced[44].

GABAergic regulation of NG2-cell development

GABA is known to be important in the regulation of neurogenesis, as GABAergic synaptic input to neuronal precursor cells promotes the survival and maturation of neuronal progenitors[11,45]. In recent studies, GABA has been shown to reduce proliferation of neuronal stem cells *via* activation of two PIKK family members – the ataxia-telangiectasia mutated (ATM) and ATM Rad 3-related (ATR) kinases – leading to the phosphorylation of the histone variant H2AX (γH2AX)[12,46]. An ability of GABA to regulate the cell cycle progression and development could also play a role in NG2-cell development.

In hippocampal NG2-cells from young rats GABA is depolarizing, due to the expression of NKCC1[39]. We found that mice lacking NKCC1 – either globally or specifically in NG2-cells – exhibited increased proliferation of cerebellar NG2-cells and a reduction in the number of mature oligodendrocytes. We have previously linked proliferation of NG2-cells and dysmyelination of the subcortical white matter following chronic hypoxia with loss of the cell cycle arrest protein p27^{KIP1} (Ref. [14]). In this regard, it is particularly interesting to note that in retinal progenitor cells, where GABA maintains proliferation, p27^{KIP1} is downregulated by $GABA_A$ receptor-mediated depolarization[47]. These results suggest that GABA-mediated depolarization in NG2-cells could provide a regulatory pathway for controlling NG2-cell development.

Our results suggest potential therapeutic avenues for promoting the repopulation of myelinating oligodendrocytes in DWMI. Thus, following hypoxia, we found that treatment with the established anti-epileptic drugs tiagabine or vigabatrin decreased the proliferation of NG2-cells and increased the number of mature oligodendrocytes to control levels. Whilst treatment of neonates with anti-epileptics may be beneficial in terms of DWMI-induced dysmyelination, our findings raise the possibility that the use of such drugs to treat infants with perinatal seizures may itself perturb myelination. This deserves investigation.

Activation of Notch signaling inhibits differentiation of oligodendrocyte precursors[48]. Recently, we have shown that intranasal EGF treatment or enhancement of epidermal growth factor receptor (EGFR) signaling in NG2-cells, by inhibiting Notch signaling, have the capacity to rescue white matter loss in DWMI[15]. Other studies have shown that overactivity in the Wnt signaling pathway following hypoxia also causes arrest in the maturation of oligodendrocyte precursors[49]. While our manuscript was in revision, a study was published that identified a role of *HIF1/2a* activity and autocrine *Wnt7a/7b* signaling in regulating OPC maturation and the response to hypoxia[50]. How these different levels of

regulation combine to determine NG2-cell proliferation and differentiation remain to be resolved. Nevertheless, our findings on the GABAergic regulation of oligodendrocyte lineage progression suggest that modulation of GABAergic signaling in DWMI may offer a complimentary approach to ameliorate the devastating effects of this currently untreatable condition.

Methods

Mice

We used NG2DsRed mice expressing the DsRed-T1 under the control of the *Ng2* promoter[51], GAD65-GFP mice (also known as *Gad2-egfp*) expressing GFP under the control of the *Gad2* promoter[52], *Nkcc1*$^{fx/fx}$ mice (also known as *Slc12a2*$^{fx/fx}$), in which the *Nkcc1* (*Slc12a2*) sequence is *loxP*-flanked [53], *Rosa26-yfp* reporter mice (Jackson Laboratories; stock number 006148) and *Pdgfra-creER*^{T2} mice that express tamoxifen-inducible Cre under the control of the *Pdgfra* promoter [54]. *Nkcc1*$^{fx/fx}$ mice were crossed with *Rosa26-yfp* mice and their offspring crossed with *Pdgfra-creER*^{T2} mice. Cre recombination produced the selective knockout of NKCC1 from NG2-cells and deletion of the *loxP*-flanked stop sequence ahead of the yellow fluorescent protein sequence enabled the persistent identification of oligodendrocyte lineage. To induce Cre recombination, tamoxifen was administered daily (P8-P11) at a dosage of 75 mg/kg body weight[15]. Genotyping was performed as previously reported[53,54]. Tissue from *NKCC1*$^{-/-}$ mice (mixed 129/SvJ and Black Swiss background) carrying a null mutation in the *Slc12a2* gene[55] were also used for immunocytochemistry. Both male and female mice were used. All procedures for the care and treatment of mice were in accordance with the National Institutes of Health Guide for the Care and Use of Laboratory Animals, the Children's National Medical Center and University of Pittsburgh Institutional Animal Care and Use Committees, and the Animals (Scientific Procedures) Act 1986. Two to four P3 pups (NG2DsRed or GAD65-GFP) were placed in a hypoxic chamber, together with two CD1 foster mothers and their pups, and exposed to 9.5–10.5% O_2 by displacing oxygen with nitrogen, as previously described[14,56,57]. At P11, mice were removed from the chamber and transferred to normoxic conditions.

BrdU administration

To assess NG2-cell proliferation, BrdU (50 mg/kg body weight) was injected intraperitoneally (i.p.) into normoxic and hypoxic NG2DsRed mice 2 hours prior to sacrifice at P11. To assess interneuron development, GAD65-EGFP mice were injected with BrdU at P8 and sacrificed at P11.

Cell cultures

Purified mouse NG2-cell cultures were prepared from P1-3 CD1 pups, as previously described [58,59]. NG2-cells were plated onto poly-L-lysine-coated coverslips and treated with 10 ng/ml platelet-derived growth factor (PDGF) (human AB, heterodimer form; Upstate Biotechnology, Lake Placid, NY). After 24 hours, cultures were treated with the $GABA_A$ receptor agonist muscimol (100 μM) (abcam) or with saline, both in the presence of the AMPA-type glutamate receptor antagonist NBQX (50 μM) (Tocris) and the NMDA receptor

antagonist D-AP5 (20 μM) (abcam). In some cases bicuculline (50 μM) was applied 1 hour prior to the administration of muscimol. After 18 hours the cells were incubated with BrdU (30 μM) (Sigma) and fixed using 4% PFA 6 hours later.

Immunocytochemistry

Immunocytochemical analysis was performed using cerebellar slices from mice at P7, 11, 15 and 30. In some cases, additional slices were examined from P60 animals. Mice were anesthetized with isoflurane and transcardially perfused with 0.1 M PBS (pH 7.4) followed by 4% paraformaldehyde, as previously described[60]. Cerebellar tissues were postfixed overnight in 4% paraformaldehyde and placed in 30% sucrose followed by 10% sucrose. Serial sagittal sections (20–50 μm thick) were cut using a cryostat microtome, collected in PBS and stored at 4°C. Immunocytochemistry was performed on free-floating sections using the following antibodies: NG2 (guinea pig, 1:500), PDGFαR (rabbit 1:500; a gift from W. B. Stallcup, Sanford-Burnham Medical Research Institute, La Jolla), Olig2 (rabbit, Millipore, ab9610, 1:200) Ki67 (rabbit, Vector labs, VP-RM04, 1:500), CC1 (mouse, Calbiochem, 444904, 1:333), MBP (mouse, Covance, SMI-94R, 1:500), NF200 (rabbit, abcam, ab82259, 1:200), Calbindin-D-28K (mouse, Sigma, C9848, 1:1000), Pax-2 (rabbit, abcam, ab37129, 1:200), BrdU (rat, abcam, ab6326, 1:250), c-caspase3 (rabbit, Cell Signaling, Asp-175, 1:200) and GFP (chicken, abcam, ab13970, 1:250). Sections were incubated overnight at 4°C in primary antibodies diluted in 0.1 M PBS (pH 7.4) containing 0.1% Triton and 5% normal goat serum. Secondary antibodies were used as follows: FITC-conjugated goat anti-mouse IgG (H+L) (Jackson Immunoresearch, 115-096-003, 1:200), Cy5-conjugated goat anti-rabbit IgG (H+L) (Jackson Immunoresearch, 111-175-144, 1:200) and Cy3 conjugated (invitrogen, A10522, 1:200). Sections were incubated with secondary antibodies for 1 hour at room temperature followed by a 10-minute incubation with DAPI (Invitrogen, D1306, 300 nM) and mounted using anti-Fade gold (Invitrogen P36930). Cultured NG2-cells were labeled with NG2 (rabbit, Millipore, MAB5384, 1:400) and BrdU (rat, Accurate Chemical, YSRTMCA2060GA, 1:100) antibodies.

Cell counting and fluorescence measurements

Four different lasers were used to image the localization of FITC (488 nm laser line excitation; 522/35 emission filter), DsRed (558 nm excitation; 583 emission), Cy5 (647 excitation; 680/32 emission) and DAPI (excitation 345; 354/400 emission).

Cell counts were obtained using 40 μm thick sagittal cerebellar sections from P7-P60 mice. Images were captured using a confocal microscope (Olympus FV1000). We consistently imaged cerebellar white matter located between the borders of the internal granule cell layers at the junction of folium VIII and IX. The white matter was first identified using a 10x objective, with DAPI stain to highlight the internal granule cell layers. The slice was then viewed using a 40x objective and images acquired with a z step size of 1 μm. The z-stack was viewed using NIH ImageJ[61] and the white matter delineated using the freehand selection tool (~50,000 μm^2). Double- or triple-labeled cells within this area were manually counted in each optical section using the ImageJ ‘Cell Counter’ plugin (ImageJ http://imagej.nih.gov/ij; http://rsb.info.nih.gov/ij/plugins/cell-counter.html). For each marker, any cells displaying immunoreactivity visually judged to be above background were scored as

positive[9]. The results were expressed as cells per 10^6 μm^3 [15]. For each condition (and littermate or vehicle controls), data were obtained from 4 to 14 mice. For each mouse, data were pooled from 4 adjacent near-midline slices.

BrdU$^+$ NG2-cells in culture were quantified using the StereoInvestigator system (http://www.mbfbioscience.com/stereo-investigator) allowing random sampling of cell counts using the optical fractionator method. Cells were counted using a 40x objective and a 3D counting frame in a sampling grid as previously described[9]. In each condition a minimum of 100 NG2-cells were counted.

Western blot analysis

Cerebellar tissue was homogenized in RIPA lysis buffer with proteinase inhibitors (Millipore 20-188). Protein extracts were boiled for 5 min before loading onto 4–20% gradient gels (GeneMate; 15 μg of protein per lane). Gels were electrotransferred to a 0.2 μm nitrocellulose membrane (Millipore). Blots were blocked in 5% milk in TBST for 1 hour, then incubated at 4°C overnight with one of the following antibodies: anti-MBP (mouse, Convance SMI-94R, 1:1000), anti-CNPase (mouse, abcam 6319, 1:1000), anti-actin (mouse, abcam ab3280, 1:1000), NF200 (rabbit, sigma 4142, 1:1000). Transferred proteins were detected with appropriate horseradish peroxide-conjugated (HRP) secondary antibodies; goat anti-mouse IgG-HRP (Santa Cruz sc-2005, 1:1000) or goat anti-rabbit IgG-HRP (Santa Cruz sc-2030, 1:1000), reacted with chemiluminescent ECL substrate (GE Healthcare), and visualized by x-ray exposure. Band intensity was measured using a calibrated densitometer (Biorad GS-800). Western blots were obtained from three animals in each group. All antibodies used in immunocytochemical or western blot analysis have been validated for use in the respective assays and species – see Antibodipedia (http://www.antibodypedia.com), CiteAb (http://www.citeab.com), suppliers' literature or Refs [15,51].

Electron microscopy

P11 mice were perfused with 4% paraformaldehyde containing 10% picric acid and 5% glutaraldehyde and the brains were removed an post-fixed for 2 weeks[15]. Cerebellar tissue sectioned (200 μm) using a slicing microtome (Leica RM2255), and postfixed in 1% osmium tetroxide in PBS for 2 hours[62]. Sagittal sections of the cerebellar white matter were examined using a Jeol transmission electron microscope (JEM 1010 or 1400). Images were acquired using a Gatan ORIUS SC1000 camera and measurements made using ImageJ. The myelin thickness was calculated from the mean of four measurements per sheath. The axon diameter was calculated from the measured circumference. The extent of myelination was compared by determining *g* ratios (the ratio of the inner axonal diameter to the total outer diameter). Measurements were performed by JS, who was blind to the origin of the tissue. At least 100 axons were measured for each brain.

Cerebellar slice preparation

Mice (P5-P11) were anesthetized with isoflurane and decapitated. After brain dissection, 250 μm thick sagittal slices were cut in an ice-cold oxygenated solution (87 mM NaCl, 2.5 mM KCl, 1.25 mM NaH_2PO_4, 7 mM $MgCl_2$, 0.5 mM $CaCl_2$, 25 mM $NaHCO_3$, 25 mM glucose, 75 mM sucrose; 347 mOsmol at pH 7.4) using a vibratome (Leica VT1000S or

Campden 7000smz). Slices were stored in the same solution at 35 °C for 30 min and then transferred into recording 'external' solution at room temperature (124 mM NaCl, 3 mM KCl, 2.5 mM $CaCl_2$, 1.3 mM $MgSO_4$, 26 mM $NaHCO_3$, 1.25 mM $NaHPO_4$, 15 mM glucose; pH 7.4 when bubbled with 95% O_2/5% CO_2).

Electrophysiology

Slices were placed in a submerged chamber on the stage of an upright microscope (Olympus BX51) and perfused at ~2 ml/min with recording solution (above). $DsRed^+$ NG2-cells and GFP^+ neurons were visualized using epifluorescence illumination and infrared differential interference contrast or infrared oblique illumination. Recording pipettes were pulled from thick-walled borosilicate glass tubing (1.5 mm outer diameter, 0.86 mm inner diameter, Harvard Apparatus) and coated with Sylgard (Dow Corning 184). For whole-cell recording, pipettes were filled with internal solution (130 mM $CsCH_3SO_3H$, 20 mM HEPES, 10 mM EGTA, 2 mM Na-ATP and 0.2 mM Na-GTP, pH 7.3) and had a resistance of 5–10 MΩ. Currents were recorded at 22–26°C using an Axopatch-200A or 700B amplifier (Molecular Devices), filtered at 5 kHz (low-pass 8-pole Bessel filter) and sampled at 10 kHz.

Recordings were made from NG2-cells and GFP^+ neurons in the white matter. NG2-cells were identified by their lack of obvious contact with neighboring fluorescent cells or blood vessels, characteristic rounded soma with few processes, and the expression of voltage-gated Na^+ channels[34]. Series resistance compensation of ~60% was applied in all whole-cell voltage-clamp recordings. For NG2-cells the final series resistance was 16.8 ± 2.1 MΩ and 21.5 ± 2.3 MΩ for normoxic and hypoxic cells (n = 31 and 29, respectively). For GFP^+ neurons the final series resistance was 18.8 ± 0.8 MΩ and 16.8 ± 1.4 MΩ for normoxic and hypoxic cells (n = 31 and 18, respectively).

Spontaneous inhibitory postsynaptic currents (sIPSCs) were recorded at +30 mV in the presence of 1 μM strychnine hydrochloride, 20 μM 6,7-dinitroquinoxaline-2,3-dione (DNQX) and 20 μM D-(−)-2-amino-5-phosphopentanoic acid (D-AP5) (Tocris Bioscience) to block glycine-, AMPA- and NMDA receptors, respectively. 5 μM QX314 (abcam) was included in the internal solution for interneuron recordings. In some recordings, extracellular stimulation (20–100 V, 20–100 μs duration at 0.1 Hz; DS2 stimulator, Digitimer) was delivered to the Purkinje cell layer using a second glass micropipette containing external solution. In all cases when tested, evoked IPSCs were fully blocked by 20 μM SR-95531 (Tocris Bioscience). mIPSCs were recorded in the additional presence of 1 μM TTX. Focal application of hyperosmotic sucrose (500 mM) was achieved using gravity-fed perfusion via a patch electrode (~1 MΩ resistance).

IPSC analysis

Records were analyzed using Igor Pro 6.10 (Wavemetrics Inc.). Spontaneous currents were detected using a scaled template algorithm based on rising and decaying exponentials[63,64] (NeuroMatic 2.6; http://www.neuromatic.thinkrandom.com/). Measurements of mean amplitude, decay and 10–90% risetime were taken from averaged events. Current decay was fitted with a double-exponential function to calculate the weighted time constant ($\tau_{w,decay}$) according to:

$$\tau_{w,decay}=\tau_f\left(\frac{A_f}{A_f+A_s}\right)+\tau_s\left(\frac{A_s}{A_f+A_s}\right) \quad (1)$$

where A_f and τ_f are the amplitude and time constant of the fast component of decay and A_s and τ_s are the amplitude and time constant of the slow component of decay. In the case of NG2 cells, to reduce errors in estimating the 10–90% risetime of relatively slow and noisy currents, individual events were fitted with an empirical equation (of the form $m^x h$):

$$f(x)=\left(1*\exp\left(-\frac{x-X0}{\tau_{rise}}\right)\right)^N*\left(A_f*\exp\left(-\frac{x-X0}{\tau_f}\right)+A_s*\exp\left(-\frac{x-X0}{\tau_s}\right)\right) \quad (2)$$

and the 10–90% risetime measured from the fitted curves[63,65].

To provide an alternative measure of GABAergic synaptic input that required no choice of parameters for the template or subjective selection of the events themselves, we also calculated the phasic charge transfer[66], using an automated procedure (written in Igor Pro). Records were divided into 5s segments and, for each, an all-point amplitude histogram was generated. The most-negative current values were then fit with a single-sided Gaussian to provide an estimate of the baseline current noise. The location of the peak of the histogram was taken as the mean baseline current value. The integral of the section of the all-point histogram not fitted by the Gaussian represents the charge carried by the phasic synaptic events. The total charge was divided by the recording time, to give a measure of phasic charge.

Purkinje cell and interneuron firing

Recordings were made from Purkinje cells visualized under infrared differential interference contrast optics. Simple spike activity was recorded at room temperature in loose cell-attached mode with external solution in the recording pipette. Spikes were detected using threshold crossing, and interspike interval (ISI), coefficient of variation of ISI (CV) and the coefficient of variation of adjacent intervals (CV2) were determined using routines written in Igor Pro[67,68]. Mean firing rate was calculated as 1/ISI. In the presence of apamin, which produced marked burst firing, modal frequency rather than mean frequency was reported. When testing the effect of carbachol on the firing of interneurons we initially recorded in whole-cell mode (at resting potential with no current injection) using an internal solution containing 150 mM potassium gluconate, 3 mM $MgCl_2$, 0.5 mM EGTA, 2 mM MgATP, 0.3 mM Na_2GTP and 10 mM HEPES; pH 7.4 with KOH. Whole-cell recording, rather than cell-attached recording, was used for interneurons, as they were not always active; this allowed us to judge the quality of the recording by first checking that the cell fired in response to current injection. Subsequently, we also made cell-attached recordings form some interneurons to test the effect of apamin. In this condition, as spontaneous firing was rare, at the end of each recording we applied carbachol to induce activity and thus verify the quality of the recording.

Drug injections

NG2DsRed mice received daily intraperitoneal (i.p.) injections (from P5-P11 or from P11-P15) of either 1 mg/kg bicuculline (abcam) in sunflower seed oil (Sigma 47123), 100 mg/kg vigabatrin in saline or 50 mg/kg tiagabine in saline (Tocris Biosciences). Control mice were injected with vehicle alone. Injection volume was 10 µl per g body weight, and solutions were warmed to 37 °C. The dose of bicuculline used was roughly half the CD_{50} reported for P7 rats[69]; two mice exhibited seizures and were excluded from the study.

Data presentation and statistical analysis

Summary data are presented in the text as mean ± s.e.m. from *n* cells or animals. Comparisons involving two data sets only were performed using a two-sided Welch two-sample *t* test that does not assume equal variance (normality was not tested statistically but gauged from Q-Q plots and/or density histograms). For Purkinje cell firing data, where we did not assume a normal distribution (Supplementary Fig. 5), a non-parametric Wilcoxon Mann-Whitney Rank Sum test was used. Analyses involving data from three or more groups were performed using one-way or two-way analysis of variance (Welch heteroscedastic *F* test) followed by pairwise comparisons using two-sided Welch two-sample *t* tests (with Holm's sequential Bonferroni correction for multiple comparisons). For analysis of contingency tables we used Fisher's exact test. Differences were considered significant at $P < 0.05$. Statistical tests were performed using Prism version 6 (GraphPad Software, Inc.) or R (version 3.0.2, The R Foundation for Statistical Computing, http://www.r-project.org/) and R Studio (version 0.98.477 RStudio, Inc.). The following packages were used: biocLite[70], car[71], coin[72] and phia[73]. No statistical test was used to predetermine sample sizes; these were based on standards of the field. No randomization was used, except in quantification of purified NG2-cells in culture (StereoInvestigator system). Blinding of investigators was used only in the EM analysis. A supplementary methods checklist is available.

Supplementary Material

Refer to Web version on PubMed Central for supplementary material.

Acknowledgments

This work was supported by the NIH (R01NS045702, P01NS062686 and P30HD040677 to VG, K08NS073793 to JS and R01NS038118 to DS), the Wellcome Trust (086185/Z/08/Z to SGC-C and MF), the MRC (MR/J002976/1 to SGC-C and MF; MR/J012998/1 to MF and SGC-C) and the DFG (HU 800/8-1 to CAU). Part of the electron microscopy was performed at the Virginia Commonwealth University Department of Anatomy and Neurobiology Microscopy Facility, supported, in part, with funding from NIH-NINDS Center core grant 5P30NS047463. MZ was in receipt of a Charlotte and Yule Bogue Research Fellowship. We thank Dwight Bergles (Johns Hopkins School of Medicine) for provision of NG2DsRed and *Pdgfra-creER*^{T2} mice, Mark Turmaine for assistance with EM and Li-Jin Chew for comments on the manuscript.

References

1. Anjari M, et al. The association of lung disease with cerebral white matter abnormalities in preterm infants. Pediatrics. 2009; 124:268–276. [PubMed: 19564309]

2. Back SA. Perinatal white matter injury: the changing spectrum of pathology and emerging insights into pathogenetic mechanisms. Ment Retard Dev Disabil Res Rev. 2006; 12:129–140. [PubMed: 16807910]
3. Allin M, et al. Cognitive maturation in preterm and term born adolescents. J Neurol Neurosurg Psychiatry. 2008; 79:381–386. [PubMed: 17682017]
4. Larroque B, et al. Neurodevelopmental disabilities and special care of 5-year-old children born before 33 weeks of gestation (the EPIPAGE study): a longitudinal cohort study. Lancet. 2008; 371:813–820. [PubMed: 18328928]
5. Kinney HC, Back SA. Human oligodendroglial development: relationship to periventricular leukomalacia. Semin Pediatr Neurol. 1998; 5:180–189. [PubMed: 9777676]
6. Back SA, et al. Late oligodendrocyte progenitors coincide with the developmental window of vulnerability for human perinatal white matter injury. J Neurosci. 2001; 21:1302–1312. [PubMed: 11160401]
7. Back SA, et al. Selective vulnerability of late oligodendrocyte progenitors to hypoxia-ischemia. J Neurosci. 2002; 22:455–463. [PubMed: 11784790]
8. Robinson S, Li Q, Dechant A, Cohen ML. Neonatal loss of gamma-aminobutyric acid pathway expression after human perinatal brain injury. J Neurosurg. 2006; 104:396–408. [PubMed: 16776375]
9. Komitova M, et al. Hypoxia-induced developmental delays of inhibitory interneurons are reversed by environmental enrichment in the postnatal mouse forebrain. J Neurosci. 2013; 33:13375–13387. [PubMed: 23946395]
10. LoTurco JJ, Owens DF, Heath MJ, Davis MB, Kriegstein AR. GABA and glutamate depolarize cortical progenitor cells and inhibit DNA synthesis. Neuron. 1995; 15:1287–1298. [PubMed: 8845153]
11. Tozuka Y, Fukuda S, Namba T, Seki T, Hisatsune T. GABAergic excitation promotes neuronal differentiation in adult hippocampal progenitor cells. Neuron. 2005; 47:803–815. [PubMed: 16157276]
12. Fernando RN, et al. Cell cycle restriction by histone H2AX limits proliferation of adult neural stem cells. Proc Natl Acad Sci U S A. 2011; 108:5837–5842. [PubMed: 21436033]
13. Liu X, Wang Q, Haydar TF, Bordey A. Nonsynaptic GABA signaling in postnatal subventricular zone controls proliferation of GFAP-expressing progenitors. Nat Neurosci. 2005; 8:1179–1187. [PubMed: 16116450]
14. Jablonska B, et al. Oligodendrocyte regeneration after neonatal hypoxia requires FoxO1-mediated p27Kip1 expression. J Neurosci. 2012; 32:14775–14793. [PubMed: 23077062]
15. Scafidi J, et al. Intranasal epidermal growth factor treatment rescues neonatal brain injury. Nature. 2014; 506:230–234. [PubMed: 24390343]
16. Lin SC, Bergles DE. Synaptic signaling between GABAergic interneurons and oligodendrocyte precursor cells in the hippocampus. Nat Neurosci. 2004; 7:24–32. [PubMed: 14661022]
17. Kukley M, et al. Glial cells are born with synapses. FASEB J. 2008; 22:2957–2969. [PubMed: 18467596]
18. Messerschmidt A, et al. Disruption of cerebellar development: potential complication of extreme prematurity. AJNR Am J Neuroradiol. 2005; 26:1659–1667. [PubMed: 16091510]
19. Pierson CR, et al. Gray matter injury associated with periventricular leukomalacia in the premature infant. Acta Neuropathol. 2007; 114:619–631. [PubMed: 17912538]
20. Nosarti C, et al. Grey and white matter distribution in very preterm adolescents mediates neurodevelopmental outcome. Brain. 2008; 131:205–217. [PubMed: 18056158]
21. Limperopoulos C, et al. Impaired trophic interactions between the cerebellum and the cerebrum among preterm infants. Pediatrics. 2005; 116:844–850. [PubMed: 16199692]
22. Buckner RL. The cerebellum and cognitive function: 25 years of insight from anatomy and neuroimaging. Neuron. 2013; 80:807–815. [PubMed: 24183029]
23. Tsai PT, et al. Autistic-like behaviour and cerebellar dysfunction in Purkinje cell Tsc1 mutant mice. Nature. 2012; 488:647–651. [PubMed: 22763451]

24. Volpe JJ. Cognitive deficits in premature infants. N Engl J Med. 1991; 325:276–278. [PubMed: 2057028]
25. Fagel DM, et al. Cortical neurogenesis enhanced by chronic perinatal hypoxia. Exp Neurol. 2006; 199:77–91. [PubMed: 15916762]
26. Scafidi J, Fagel DM, Ment LR, Vaccarino FM. Modeling premature brain injury and recovery. Int J Dev Neurosci. 2009; 27:863–871. [PubMed: 19482072]
27. Barres BA, Raff MC. Proliferation of oligodendrocyte precursor cells depends on electrical activity in axons. Nature. 1993; 361:258–260. [PubMed: 8093806]
28. Calver AR, et al. Oligodendrocyte population dynamics and the role of PDGF in vivo. Neuron. 1998; 20:869–882. [PubMed: 9620692]
29. Bergles DE, Roberts JD, Somogyi P, Jahr CE. Glutamatergic synapses on oligodendrocyte precursor cells in the hippocampus. Nature. 2000; 405:187–191. [PubMed: 10821275]
30. Mangin JM, Kunze A, Chittajallu R, Gallo V. Satellite NG2 progenitor cells share common glutamatergic inputs with associated interneurons in the mouse dentate gyrus. J Neurosci. 2008; 28:7610–7623. [PubMed: 18650338]
31. Velez-Fort M, Maldonado PP, Butt AM, Audinat E, Angulo MC. Postnatal switch from synaptic to extrasynaptic transmission between interneurons and NG2 cells. J Neurosci. 2010; 30:6921–6929. [PubMed: 20484634]
32. Karadottir R, Hamilton NB, Bakiri Y, Attwell D. Spiking and nonspiking classes of oligodendrocyte precursor glia in CNS white matter. Nat Neurosci. 2008; 11:450–456. [PubMed: 18311136]
33. Maricich SM, Herrup K. Pax-2 expression defines a subset of GABAergic interneurons and their precursors in the developing murine cerebellum. J Neurobiol. 1999; 41:281–294. [PubMed: 10512984]
34. De Biase LM, Nishiyama A, Bergles DE. Excitability and synaptic communication within the oligodendrocyte lineage. J Neurosci. 2010; 30:3600–3611. [PubMed: 20219994]
35. Simat M, Ambrosetti L, Lardi-Studler B, Fritschy JM. GABAergic synaptogenesis marks the onset of differentiation of basket and stellate cells in mouse cerebellum. Eur J Neurosci. 2007; 26:2239–2256. [PubMed: 17892480]
36. Pitler TA, Alger BE. Depolarization-induced suppression of GABAergic inhibition in rat hippocampal pyramidal cells: G protein involvement in a presynaptic mechanism. Neuron. 1994; 13:1447–1455. [PubMed: 7993636]
37. Deshmukh VA, et al. A regenerative approach to the treatment of multiple sclerosis. Nature. 2013; 502:327–332. [PubMed: 24107995]
38. Ge S, et al. GABA regulates synaptic integration of newly generated neurons in the adult brain. Nature. 2006; 439:589–593. [PubMed: 16341203]
39. Tong XP, et al. Ca(2+) signaling evoked by activation of Na(+) channels and Na(+)/Ca(2+) exchangers is required for GABA-induced NG2 cell migration. J Cell Biol. 2009; 186:113–128. [PubMed: 19596850]
40. Foran DR, Peterson AC. Myelin acquisition in the central nervous system of the mouse revealed by an MBP-Lac Z transgene. J Neurosci. 1992; 12:4890–4897. [PubMed: 1281497]
41. Lee Y, et al. The genesis of cerebellar interneurons and the prevention of neural DNA damage require XRCC1. Nat Neurosci. 2009; 12:973–980. [PubMed: 19633665]
42. Glickstein SB, et al. Selective cortical interneuron and GABA deficits in cyclin D2-null mice. Development. 2007; 134:4083–4093. [PubMed: 17965053]
43. Nguyen MV, et al. Oligodendrocyte lineage cells contribute unique features to Rett syndrome neuropathology. J Neurosci. 2013; 33:18764–18774. [PubMed: 24285883]
44. Chao HT, et al. Dysfunction in GABA signalling mediates autism-like stereotypies and Rett syndrome phenotypes. Nature. 2010; 468:263–269. [PubMed: 21068835]
45. Song J, et al. Parvalbumin interneurons mediate neuronal circuitry-neurogenesis coupling in the adult hippocampus. Nat Neurosci. 2013; 16:1728–1730. [PubMed: 24212671]
46. Andang M, et al. Histone H2AX-dependent GABA(A) receptor regulation of stem cell proliferation. Nature. 2008; 451:460–464. [PubMed: 18185516]

47. Ring H, Mendu SK, Shirazi-Fard S, Birnir B, Hallbook F. GABA maintains the proliferation of progenitors in the developing chick ciliary marginal zone and non-pigmented ciliary epithelium. PLoS One. 2012; 7:e36874. [PubMed: 22590629]
48. Wang S, et al. Notch receptor activation inhibits oligodendrocyte differentiation. Neuron. 1998; 21:63–75. [PubMed: 9697852]
49. Fancy SP, et al. Parallel states of pathological Wnt signaling in neonatal brain injury and colon cancer. Nat Neurosci. 2014; 17:506–512. [PubMed: 24609463]
50. Yuen TJ, et al. Oligodendrocyte-encoded HIF function couples postnatal myelination and white matter angiogenesis. Cell. 2014; 158:383–396. [PubMed: 25018103]
51. Zhu X, Bergles DE, Nishiyama A. NG2 cells generate both oligodendrocytes and gray matter astrocytes. Development. 2008; 135:145–157. [PubMed: 18045844]
52. Lopez-Bendito G, et al. Preferential origin and layer destination of GAD65-GFP cortical interneurons. Cereb Cortex. 2004; 14:1122–1133. [PubMed: 15115742]
53. Antoine MW, Hubner CA, Arezzo JC, Hebert JM. A causative link between inner ear defects and long-term striatal dysfunction. Science. 2013; 341:1120–1123. [PubMed: 24009395]
54. Kang SH, Fukaya M, Yang JK, Rothstein JD, Bergles DE. NG2+ CNS glial progenitors remain committed to the oligodendrocyte lineage in postnatal life and following neurodegeneration. Neuron. 2010; 68:668–681. [PubMed: 21092857]
55. Flagella M, et al. Mice lacking the basolateral Na-K-2Cl cotransporter have impaired epithelial chloride secretion and are profoundly deaf. J Biol Chem. 1999; 274:26946–26955. [PubMed: 10480906]
56. Bi B, et al. Cortical glial fibrillary acidic protein-positive cells generate neurons after perinatal hypoxic injury. J Neurosci. 2011; 31:9205–9221. [PubMed: 21697371]
57. Raymond M, Li P, Mangin JM, Huntsman M, Gallo V. Chronic perinatal hypoxia reduces glutamate-aspartate transporter function in astrocytes through the Janus kinase/signal transducer and activator of transcription pathway. J Neurosci. 2011; 31:17864–17871. [PubMed: 22159101]
58. Ghiani CA, et al. Voltage-activated K+ channels and membrane depolarization regulate accumulation of the cyclin-dependent kinase inhibitors p27(Kip1) and p21(CIP1) in glial progenitor cells. J Neurosci. 1999; 19:5380–5392. [PubMed: 10377348]
59. Chen Y, et al. Isolation and culture of rat and mouse oligodendrocyte precursor cells. Nat Protoc. 2007; 2:1044–1051. [PubMed: 17546009]
60. Mangin JM, Li P, Scafidi J, Gallo V. Experience-dependent regulation of NG2 progenitors in the developing barrel cortex. Nat Neurosci. 2012; 15:1192–1194. [PubMed: 22885848]
61. Schneider CA, Rasband WS, Eliceiri KW. NIH Image to ImageJ: 25 years of image analysis. Nat Methods. 2012; 9:671–675. [PubMed: 22930834]
62. Pacey LK, et al. Delayed myelination in a mouse model of fragile X syndrome. Hum Mol Genet. 2013; 22:3920–3930. [PubMed: 23740941]
63. Bekkers JM, Stevens CF. Cable properties of cultured hippocampal neurons determined from sucrose-evoked miniature EPSCs. J Neurophysiol. 1996; 75:1250–1255. [PubMed: 8867133]
64. Clements JD, Bekkers JM. Detection of spontaneous synaptic events with an optimally scaled template. Biophys J. 1997; 73:220–229. [PubMed: 9199786]
65. Bekkers JM, Clements JD. Quantal amplitude and quantal variance of strontium-induced asynchronous EPSCs in rat dentate granule neurons. J Physiol. 1999; 516 (Pt 1):227–248. [PubMed: 10066937]
66. Glykys J, Mody I. The main source of ambient GABA responsible for tonic inhibition in the mouse hippocampus. J Physiol. 2007; 582:1163–1178. [PubMed: 17525114]
67. Hausser M, Clark BA. Tonic synaptic inhibition modulates neuronal output pattern and spatiotemporal synaptic integration. Neuron. 1997; 19:665–678. [PubMed: 9331356]
68. Wulff P, et al. Synaptic inhibition of Purkinje cells mediates consolidation of vestibulo-cerebellar motor learning. Nat Neurosci. 2009; 12:1042–1049. [PubMed: 19578381]
69. Baram TZ, Snead OC 3rd. Bicuculline induced seizures in infant rats: ontogeny of behavioral and electrocortical phenomena. Brain Res Dev Brain Res. 1990; 57:291–295. [PubMed: 2073726]

70. Pollard KS, Gilbert HN, Ge Y, Taylor S, Dudoit S. multtest: Resampling-based multiple hypothesis testing. R package version 2.18.0.
71. Fox, J.; Weisberg, S. An {R} Companion to Applied Regression. Sage; Thousand Oaks CA: 2011.
72. Hothorn T, Hornik K, van de Wiel MA, Zeileis A. A Lego System for Conditional Inference. The American Statistician. 2006; 60:257–263.
73. De Rosario-Martinez H. phia: Post-Hoc Interaction Analysis. R package version 0.1-5. 2013

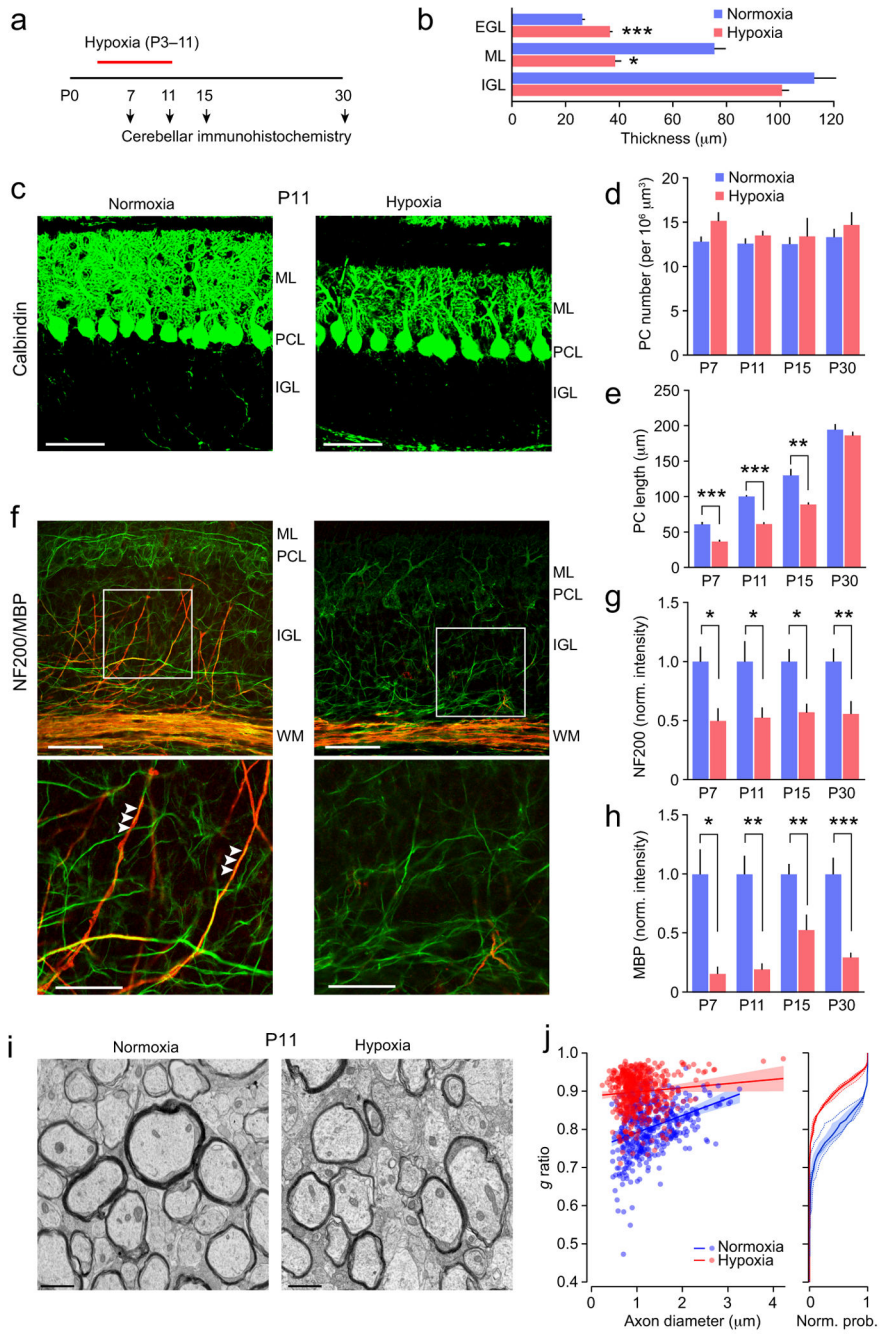

Figure 1. Changes in cerebellar myelination following neonatal hypoxia

(**a**) Timeline showing the experimental design. (**b**) Effect of hypoxia on thickness of cortical layers at P11. Note the lack of change in internal granule cell layer (IGL; $n = 4$ mice each), but reduced thickness of the molecular layer (ML; $n = 6$ and 5 mice) and increased thickness of the external granule cell layer (EGL; $n = 6$ and 5 mice). For all panels bar graphs are presented as mean ± s.e.m. * $P < 0.05$, ** $P < 0.01$, *** $P < 0.001$ (unpaired Welch two-sample *t* tests). (**c**) Representative confocal images of sagittal sections from P11 mice showing calbindin immunofluorescence (green). ML, molecular layer; PCL, Purkinje cell

layer; IGL, internal granule cell layer. Scale bars 50 μm. (**d**) Effects of hypoxic treatment on Purkinje cell (PC) number. Two-way ANOVA showed a significant main effect of treatment but no effect of age and no interaction between age and treatment (n = 4–7 normoxic mice and 4–7 hypoxic mice). There was no effect of hypoxia on Purkinje cell number at any age. (**e**) Hypoxic treatment decreased Purkinje cell length at P7-P15. Two-way ANOVA showed significant main effects of hypoxia and age and a significant interaction (n = 4–7 normoxic mice and 5 hypoxic mice at each age). (**f**) Representative confocal images showing NF200 (green) and MBP (red) immunofluorescence. Abbreviations are as in c, plus WM, white matter. Scale bars 50 μm. Boxed areas are shown enlarged in lower row. Scale bars 25 μm. Arrowheads indicate myelination of presumptive Purkinje cell axons. Note the reduced myelination of these axons following hypoxia. (**g**) Hypoxic treatment decreased NF200 immunofluorescence in white matter. Two-way ANOVA showed a significant effect of hypoxia, no significant effect of age and no interaction (n = 6–10 normoxic mice and 5–12 hypoxic mice). (**h**) Hypoxic treatment decreased MBP immunofluorescence in white matter. Two-way ANOVA showed significant effects of hypoxia, no effect of age and no interaction (n = 5–10 normoxic mice and 4–9 hypoxic mice). (**i**) Electron microscopy images from P11 white matter. Scale bars 1 μm. (**j**) Left, scatter plot of g ratios of individual axons versus axon diameter; pooled data from three normoxic and three hypoxic mice (blue and red, respectively). Fitted lines are linear regressions and shaded areas indicate 95% confidence bands. Right, plot of normalized cumulative probability of g ratio for the 3 normoxic mice (blue dashed lines) and the three hypoxic mice (red dashed lines). Solid lines are the averaged probability plots and the shaded areas denote the s.e.m. Hypoxia increased the g ratio from 0.81 ± 0.02 to 0.91 ± 0.004. See Supplementary Methods Checklist for full details of statistical tests.

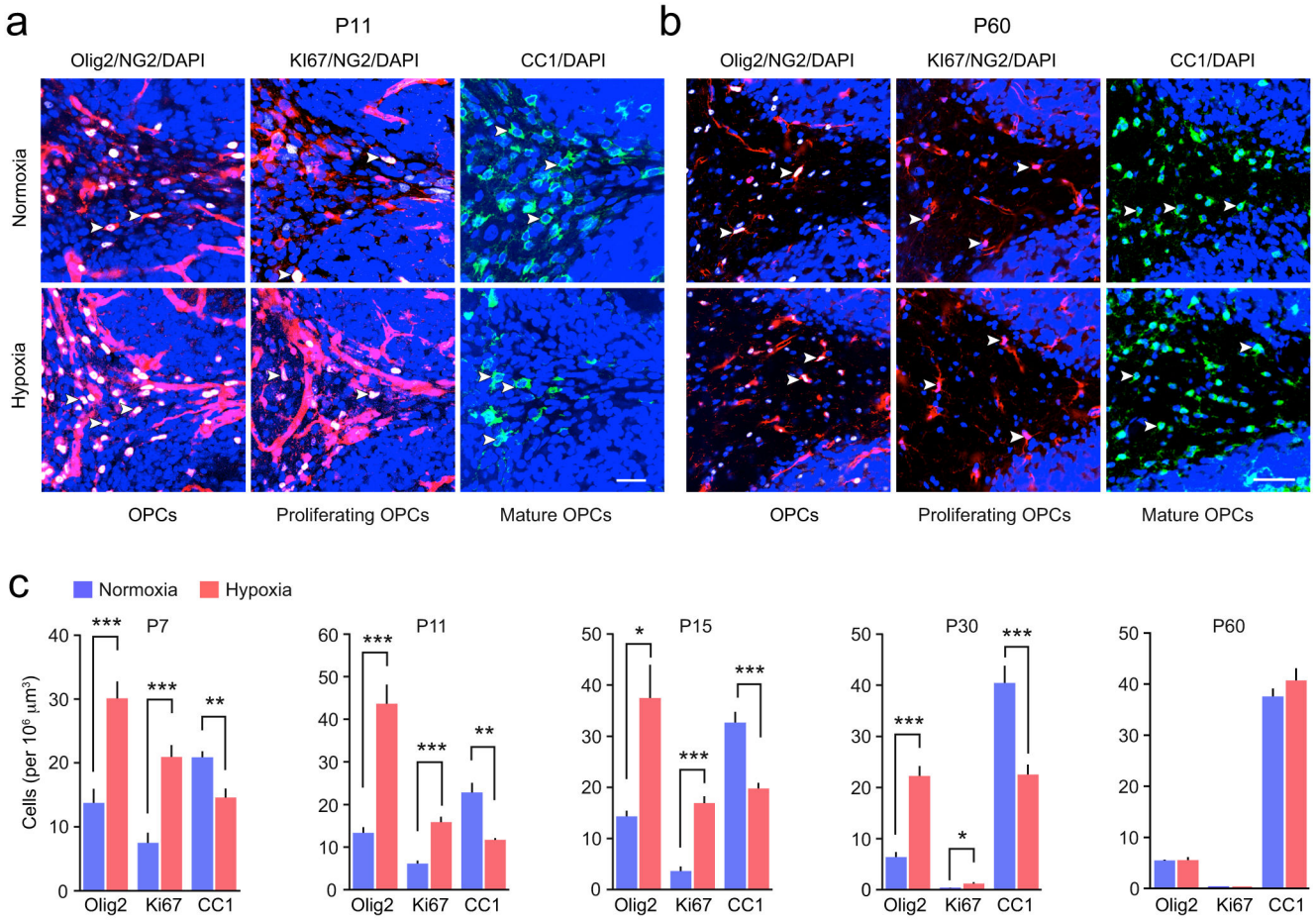

Figure 2. Altered development of NG2-cells following neonatal hypoxia

(**a**) Representative confocal images of sagittal sections of cerebellar white matter from NG2DsRed mice at P11. NG2-cells (red) were co-labeled with Olig2 (an oligodendrocyte lineage marker; white), Ki67 (a marker of proliferation; white), CC1 (a marker of mature oligodendrocytes; green) and DAPI (blue). Yellow arrowheads indicate selected triple-labeled NG2-cells and double-labeled $CC1^+$ cells. Scale bar 25 µm. (**b**) Representative images as shown in a, but from P60 mice. Scale bar 50 µm. (**c**) Pooled data showing the effect of hypoxia on the numbers of $Olig2^+/NG2^+$-, $Ki67^+/NG2^+$- and $CC1^+$ cells. Graphs are presented as mean ± s.e.m. * $P < 0.05$, ** $P < 0.01$, *** $P < 0.001$ (unpaired Welch two-sample *t* tests; n = 5–10, 6–9, 8–6, 4–14, and 3 mice at P7, 11, 15, 30 and 60, respectively). See Supplementary Methods Checklist for full details of statistical tests.

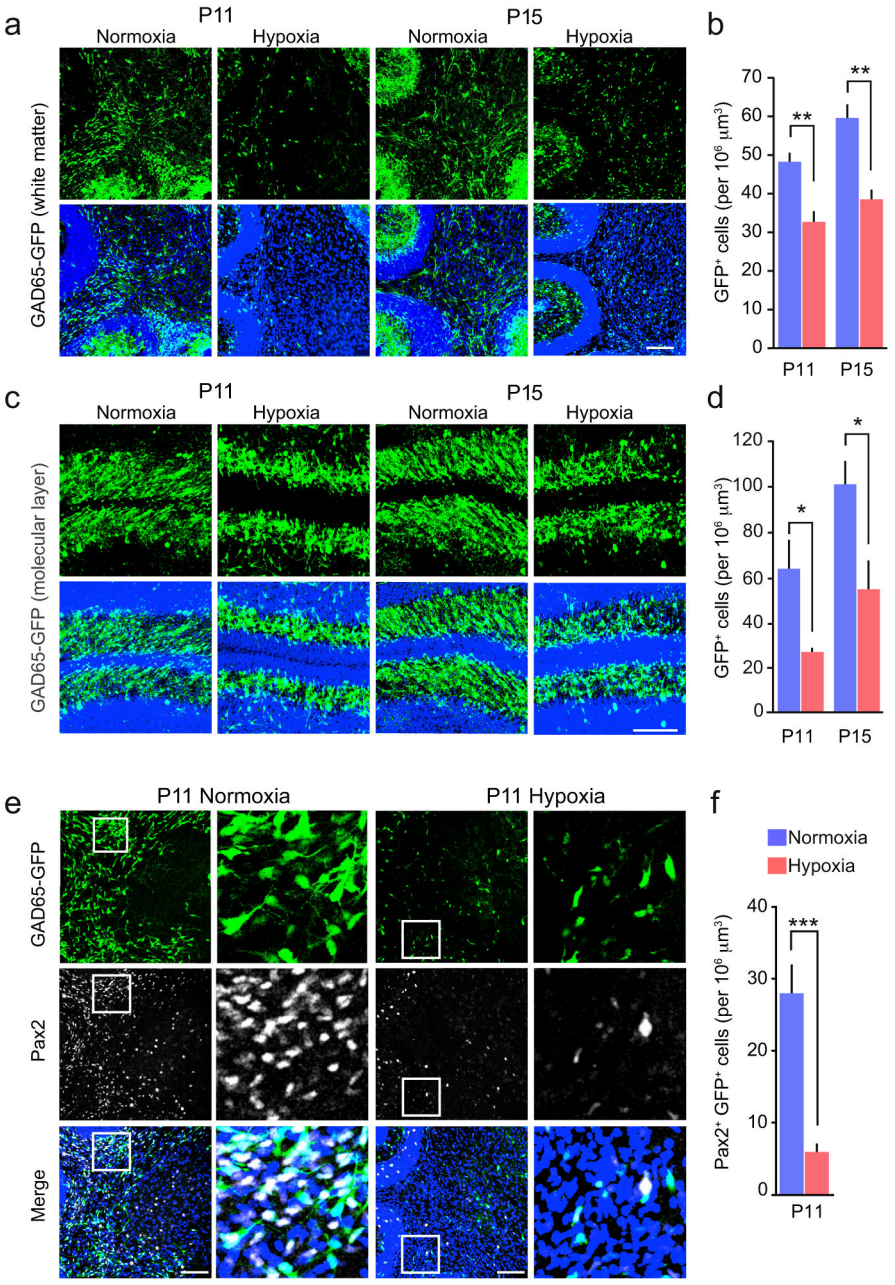

Figure 3. Loss of cerebellar GABAergic neurons following neonatal hypoxia

(**a**) Representative confocal images of sagittal cerebellar sections from GAD65-GFP mice showing GAD65 expressing neurons (green) in the white matter of normoxic and hypoxic littermates at P11 and P15. Lower panels show merged images with DAPI (blue). Scale bars 200 µm. (**b**) Pooled data showing the effect of hypoxic treatment on the number of cerebellar white matter GAD65$^+$ neurons. (*n* = 5 and 4 mice at P11 and 5 mice each at P15). (**c**, **d**) Same as shown in a and b, for molecular layer (*n* = 5 mice each at P11 and 6 and 5 mice at P15). (**e**) Representative confocal images from P11 mice showing expression of the transcription factor Pax2 (white; middle) in GAD65$^+$ neurons (green; upper). Lower panels show merged images with DAPI (blue). Scale bars 200 µm. Selected regions of white matter

(boxed) are enlarged to the right. (**f**) Pooled data showing the effect of hypoxic treatment on the number of $Pax2^{+}$ GAD65-GFP cells in the white matter at P11 (n = 11 and 12 mice). All graphs are presented as mean ± s.e.m. * $P < 0.05$, ** $P < 0.01$, *** $P < 0.001$ (unpaired Welch two-sample t tests). See Supplementary Methods Checklist for full details of statistical tests.

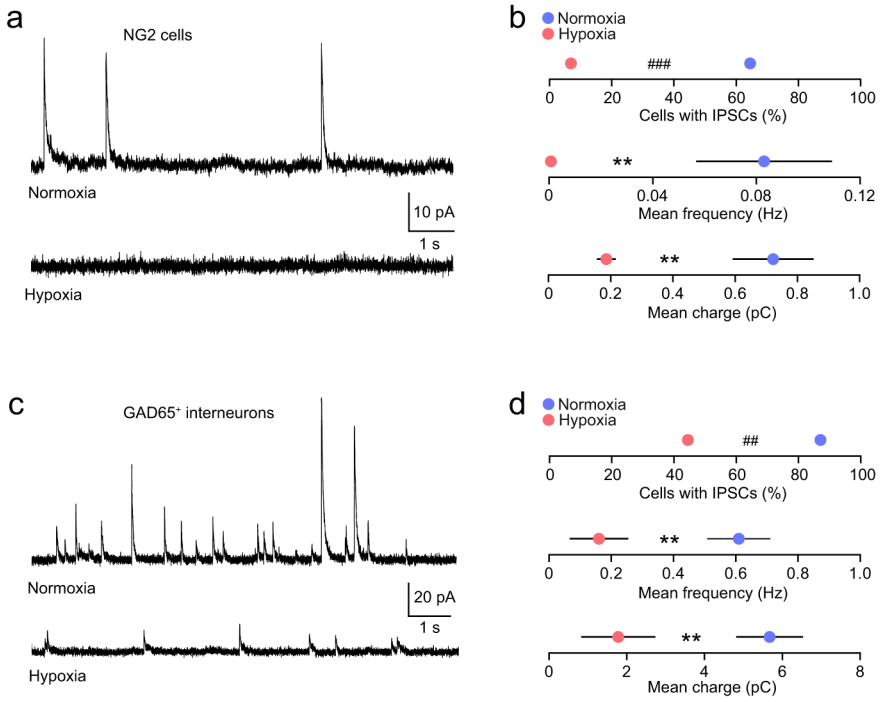

Figure 4. Reduced GABAergic synaptic activity in cerebellar white matter NG2-cells and GABAergic interneurons following neonatal hypoxia

(**a**) Representative whole-cell current recordings from cerebellar white matter NG2-cells (+30 mV) in slices from a control NG2DsRed mouse (upper trace, P8) and from a mouse following hypoxic treatment (lower trace, P7). (**b**) Pooled data showing reduced IPSC prevalence (20/31 cells from 13 normoxic mice and 2/29 cells from 9 hypoxic mice; $^{###}P < 0.001$, Fisher's exact test), reduced IPSC frequency and reduced IPSC-mediated charge transfer following hypoxia (** $P < 0.01$; unpaired Welch two sample *t* tests). (**c**) Representative whole-cell current recordings from cerebellar white matter GAD65^{+} neurons (+30 mV) in slices from a control mouse (upper trace, P8) and from a mouse following hypoxic treatment (lower trace, P9). (**d**) Pooled data showing reduced IPSC prevalence (27/31 cells from 10 normoxic mice and 8/18 cells from 7 hypoxic mice; $^{##}P < 0.01$, Fisher's exact test), reduced IPSC frequency and reduced IPSC-mediated charge transfer following hypoxia (** $P < 0.01$; unpaired Welch two sample *t* tests). Frequency and charge data shown as mean ± s.e.m. See Supplementary Methods Checklist for full details of statistical tests.

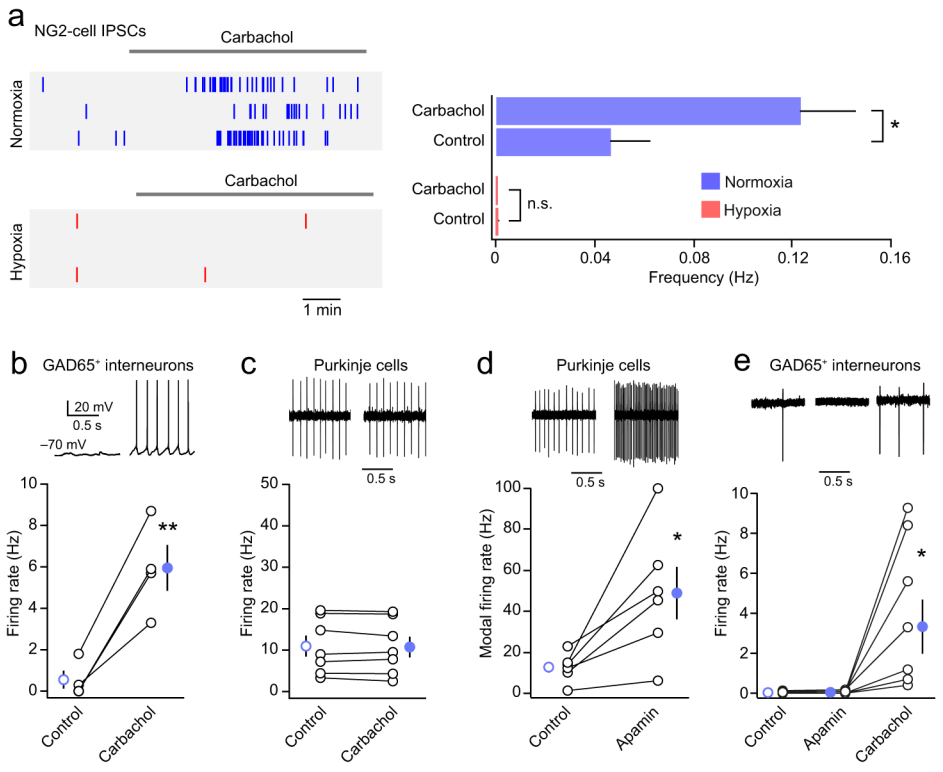

Figure 5. The carbachol-induced increase in NG2-cell sIPSC frequency reflects an increased activity of local white matter interneurons

(**a**) Left, raster plots illustrating the increase in the frequency of spontaneous IPSCs induced by carbachol (10 μM) in NG2-cells in slices from normoxic NG2DsRed mice (upper panel). The lower panel illustrates the lack of effect of carbachol in slices taken from animals following hypoxic treatment. In each case, three representative cells are illustrated. Right, bar plot showing pooled data from normoxic and hypoxic mice (n = 15 cells from 11 mice and 14 cells from 6 mice, respectively). (**b**) Summary plot showing that carbachol (10 μM) increased the firing of white matter GAD65$^+$ interneurons (n = 4 cells from 3 mice). Inset: representative episodes from a whole-cell recording from a P9 interneuron before and after carbachol treatment (initial resting potential shown; no current injection). (**c**) Carbachol (10 μM) had no effect on the mean firing rate of Purkinje cells (n = 7 cells from 3 mice). Inset: representative cell-attached recordings from a P8 Purkinje cell obtained before and 5 mins after bath application of carbachol. (**d**) Apamin (100 nM) increased Purkinje cell firing (n = 6 cells from 3 mice). Inset: representative cell-attached recordings from a P8 Purkinje cell obtained before and 6 mins after bath application of apamin. (**e**) Apamin (100 nM) did not increase the firing of white matter GAD65$^+$ interneurons, while, in each case, subsequent application of carbachol (10 μM) did (n = 9 cells from 9 mice). Inset: representative cell-attached recordings from a P8 interneuron obtained before drug application, 2 mins after bath application of apamin, and 1 min after bath application of carbachol. Graphs show mean ± s.e.m.; * $P < 0.05$, ** $P < 0.01$, paired Welch two sample t tests. See Supplementary Methods Checklist for full details of statistical tests.

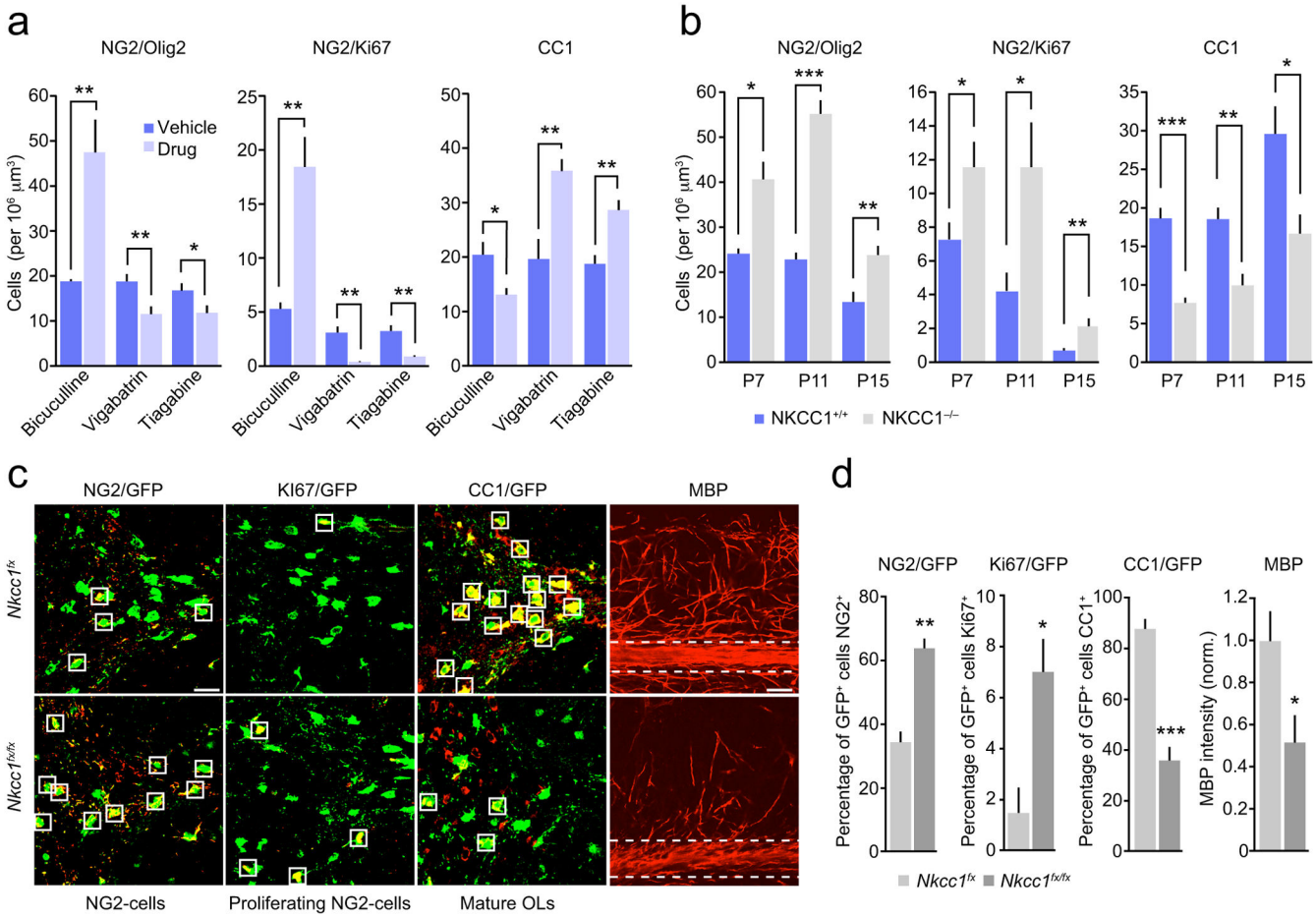

Figure 6. Modulation of cerebellar white matter NG2-cell development by GABAergic drugs and NKCC1 deletion

(**a**) Pooled data showing that bicuculline increased the proliferation of Olig2$^+$ and Ki67$^+$ NG2-cells, whilst decreasing the number of CC1$^+$ cells and that both vigabatrin and tiagabine produced opposite effects to bicuculline (*n* = 4–10 mice each) (see Supplementary Methods Checklist for details). (**b**) Pooled data showing the effects of the deletion of NKCC1 on numbers of Olig2$^+$ and KI67$^+$ NG2-cells and CC1$^+$ cells at P7, 11 and 15 (*n* = 3–6 mice each) (see Supplementary Methods Checklist and Supplementary Fig. 8 for representative images). (**c**) Representative confocal images of cerebellar white matter from P15 *Pdgfra-creER^{T2}*;*Nkcc1^{fx}*;*Rosa26-yfp* mice (heterozygote control; *Nkcc1^{fx}*) and *Pdgfra-creER^{T2}*; *Nkcc1$^{fx/fx}$*;*Rosa26-yfp* mice (homozygote knockout; *Nkcc1$^{fx/fx}$*). NG2-cells in which Cre was activated were YFP$^+$ and were labeled with GFP antibody (green). Sections were co-labeled with NG2 (red), Ki67 (white) or CC1 (red). Right hand columns show MBP (red) alone. Scale bar 50 µm. Box outlines indicate example GFP$^+$ cells, which are positive for NG2, Ki67 or CC1. For MBP immunolabeling (right columns) horizontal dashed lines indicate white matter areas where MBP was measured. (**d**) Pooled data demonstrating the effect of NG2-cell-specific NKCC1 deletion on the percentage of NG2$^+$, Ki67$^+$ and CC1$^+$ GFP$^+$ oligodendrocyte lineage cells, and the effect on MBP labeling in the white matter (*n* =

4 *Nkcc1*^{fx} and $n = 4$ *Nkcc1*$^{fx/fx}$) (see Supplementary Methods Checklist). Graphs are presented as mean ± s.e.m. * $P < 0.05$, ** $P < 0.01$ (unpaired Welch two-sample *t* tests).

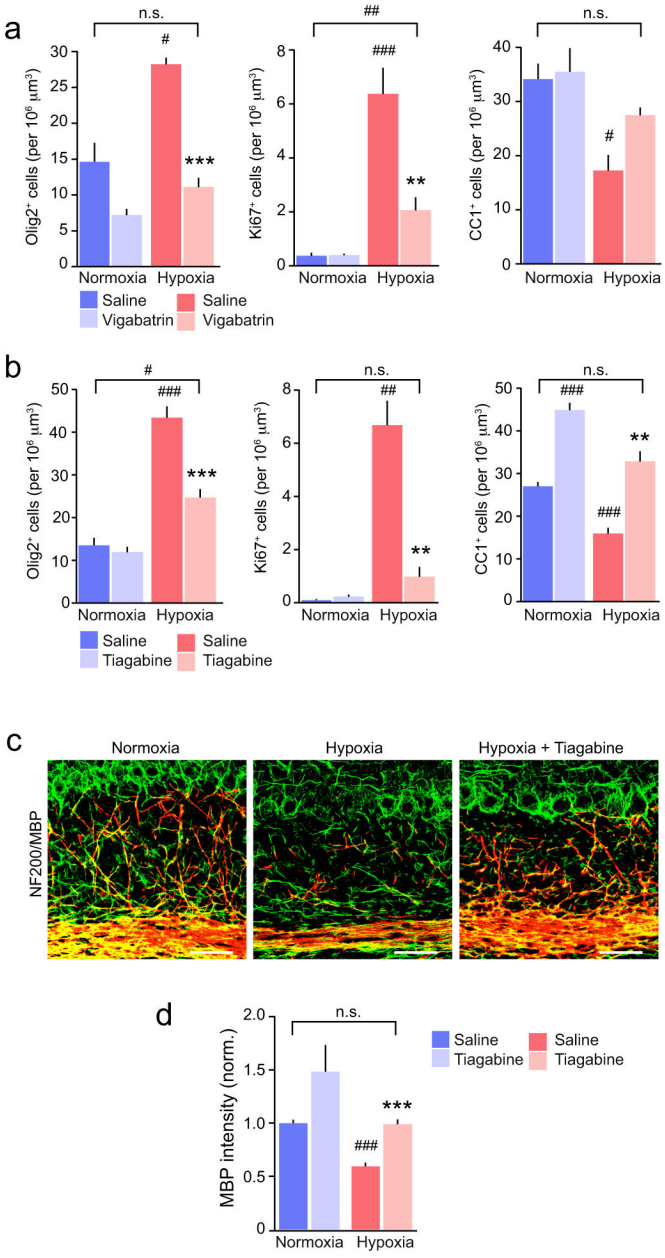

Figure 7. Effects of tiagabine and vigabatrin on NG2-cell proliferation and loss of mature oligodendrocytes following hypoxia

(**a**) Pooled data showing the effects of vigabatrin (n = 4–10 mice) on the numbers of Olig2$^+$, Ki67$^+$ and CC1$^+$ cells. Details of animal numbers and results of two-way ANOVA are presented in Supplementary Methods Checklist (see Supplementary Fig. 8 for representative images). (**b**) Same as shown in a, but for tiagabine (n = 4–7 mice). Asterisks denote the significance of differences between saline and drug in hypoxic mice (* $P < 0.05$, ** $P < 0.01$, *** $P < 0.001$), and hash symbols denote the significance of differences between all conditions and normoxic saline-injected controls ($^{\#}P < 0.05$, $^{\#\#}P < 0.01$, $^{\#\#\#}P < 0.001$; Welch two sample unpaired t test with Holm's sequential Bonferroni correction for repeated tests; for details see Supplementary Methods Checklist). (**c**) Representative confocal images

showing NF200 (green) and MBP (red) in cerebellar sections from P15 saline-treated normoxic mice and hypoxic mice treated with either with saline or tiagabine. Scale bars 50 μm. (**d**) Pooled data (n = 5–6 mice) showing that following hypoxia, tiagabine (P11 to P15) promoted recovery of MBP. Asterisks and hash symbols as defined in b; for details see Supplementary Methods Checklist. Graphs are presented as mean ± s.e.m.